Results in Engineering 30 (2026) 110860

Contents lists available at ScienceDirect

Results in Engineering

journal homepage: www.sciencedirect.com/journal/results-in-engineering

Research paper

Measurement based data-driven modeling of a thermoelectric generator (TEG)

Károly Árpád Kis, Kornél Sarvajcz, Róbert Mikuska *, Péter Korondi

University of Debrecen, Faculty of Engineering, Department of Electrical Engineering and Mechatronics, Ótemető utca 2–4., Debrecen, 4028, Hungary

ARTICLE INFO

Keywords:
Thermoelectric generator (TEG)
Renewable energy system
Bacterial memetic algorithm (BMA)
Parameter identification
Fuzzy model
TP model

ABSTRACT

Due to the complex physical behavior of thermoelectric generators (TEGs), direct physics-based modeling is often impractical. The main contribution of this research is that three different data-driven models are made for three different objectives. The first method is a classical parametric curve fitting technique using parameter identification based Bacterial Memetic Algorithm (BMA). The second is a fuzzy model with arbitrarily defined trapezoidal membership functions, where the anchor points are optimized using BMA as well. The third approach is a tensor product (TP) model transformation based polytopic model. The study provides a comparative analysis of these approaches, emphasizing their modeling flexibility and accuracy in representing the nonlinear characteristics of TEGs.

1. Introduction

It probably goes without saying that all kinds of green and/or renewable energy systems are hugely popular these days. Energy harvesting systems are no different.

1.1. State of the art: Thermal-based energy harvesting for vehicles

Thermoelectric generators (TEGs) offer a promising solution for recovering waste heat in vehicles by directly converting thermal energy into electrical power via the Seebeck effect. Recent advancements have focused on optimizing TEG configurations, improving efficiency, and integrating them into various vehicle types.

Lan et al. optimized the electrical load resistance and configuration of a TEG for electric vehicles, achieving an 11.6% increase in net power density [1]. They further compared simulation and real-world results for TEGs in internal combustion and electric vehicles [2]. Nader explored fuel-saving potential in hybrid electric vehicles [3], while Mohamed et al. simulated low-grade waste heat recovery [4]. Luo et al. developed a multiphysics numerical model to predict TEG performance [5], and Abbasi et al. introduced a flexible measurement system for vehicle temperature monitoring [6].

Sousa et al. optimized a temperature-controlled TEG for heavy-duty vehicles [7]. Coulibaly et al. investigated TEGs for braking heat recovery [8], and Aljaghtham et al. applied multiphysics simulations to heat conversion from an oil tank [9]. Dalkiranis et al. developed a low cost device to obtain the Seebeck coefficient and electrical conductivity of thermoelectric materials [10]. Atmajaya et al. developed a TEG for diesel engine heat recycling [11], while Olabi et al. explored TEG integration with other sustainable technologies [12]. Khoshnevisan et al. dynamically designed a hybrid vehicle with TEGs [13], and Kumar et al. analyzed exhaust heat recovery [14]. He et al. propose a framework to predict the remaining useful life of the device [15]. Other studies investigated TEGs in motorcycles [16], thermal management strategies [17], and multi-stage energy extraction [18]. Comprehensive reviews on TEG technology can be found in [19–21].

1.2. The thermoelectric generator (TEG)

TEGs operate on the Seebeck effect, where a temperature gradient across n-type and p-type semiconductors generates electric current. These compact, reliable devices require no moving parts and are widely used in heat recovery applications. Their efficiency depends on material properties, temperature gradients, and thermal/electrical conductivity.

A typical TEG consists of an n-type and a p-type semiconductor, with copper as a conductive contact. Bismuth Telluride (Bi_2Te_3) is the most common semiconductor due to its superior thermoelectric properties. The assembly is sandwiched between ceramic insulating layers like aluminum oxide (Al_2O_3) [22].

TEG operation involves three primary thermoelectric effects: (1) the Seebeck effect, generating voltage from a temperature gradient; (2) the Peltier effect, where current flow causes heating or cooling at junctions;

* Corresponding author.
E-mail addresses: kis.karoly@eng.unideb.hu (K.Á. Kis), sarvajcz@eng.unideb.hu (K. Sarvajcz), mikuska.robert@eng.unideb.hu (R. Mikuska), korondi.peter@eng.unideb.hu (P. Korondi).

https://doi.org/10.1016/j.rineng.2026.110860
Received 23 March 2026; Received in revised form 16 April 2026; Accepted 2 May 2026
Available online 5 May 2026

and (3) the Thomson effect, which describes heat dissipation in conductors with temperature variations.

1.3. Parameter identification by machine learning

Parameter identification is a fundamental process in many scientific and engineering domains, as it enables the accurate characterization of complex systems. Traditional analytical methods often struggle to model non-linear relationships or dynamic behaviors in real-world systems, leading to limited accuracy. Machine learning techniques offer a data-driven approach to parameter identification, overcoming these challenges by learning patterns directly from data.

Machine learning provides tools to build models that can analyze input-output relationships and predict system behavior under various conditions. This approach is particularly effective for systems where underlying dependencies are difficult to capture using conventional methods. The flexibility of machine learning allows it to handle noisy data and adapt to changing system dynamics, making it an essential method for modern parameter identification tasks.

To enhance the precision and efficiency of machine learning-based parameter estimation, advanced optimization algorithms, such as the Bacterial Memetic Algorithm (BMA), are often employed. These hybrid algorithms combine global search methods with local refinement techniques to achieve optimal solutions. By integrating machine learning and optimization, parameter identification becomes a powerful and versatile tool for improving system performance and reliability across diverse applications.

1.4. Brief overview of the bacterial memetic algorithm

Several evolutionary optimization algorithms have been developed that are able to solve and quasi-optimise problems with non-linear and non-continuous characteristics [23,24]. The Bacterial Evolutionary Algorithm (BEA) [25] is one of the options that mimic bacterial rather than eukaryotic evolution. Each bacterium is a solution to the original problem. In bacterial mutation and gene transfer, bacteria share pieces of their genes, rather than performing a pure cross between chromosomes, which is typical of eukaryotes. The main disadvantage of classical evolutionary algorithms is their low convergence rate and hence long runtimes. However, by combining them with gradient-based local search methods, the advantages of both methods can be exploited in the optimization process. This hybridization leads to memetic algorithms [26].

The BMA [27] is a memetic algorithm in which the bacterial technique is used instead of the classical genetic algorithm, with the Levenberg-Marquardt (LM) method [28,29] as the local search method. BMA provides competitive performance in optimization [30,31] and supervised machine learning [31] over genetic algorithm (GA) and particle swarm optimization (PSO) and their memetic variants. It has been applied to a number of combinatorial optimization problems [30,32] in continuous optimization problems [33], and in supervised machine learning problems such as fuzzy rule base extraction [27] and fuzzy neural network training [34].

Many successful optimization methods are gradient-based, usually described as local methods. This locality is the main source of their advantages and disadvantages. Their convergence is fast, but they may get stuck in the local optimum. Evolutionary algorithms (EA) are used to solve complex and non-linear problems. A common characteristic of all evolutionary algorithms is that several possible solutions compete for survival in the population. They are globally explored, but convergence is slow near the optimum. However, due to the limitations associated with them [35], several hybrid computational techniques have been developed that remain global and explore large search spaces, with local search increasing convergence speed. The main steps in most evolutionary algorithms are selection, crossover, and mutation.

Memetic algorithms combine the advantages of evolutionary algorithms and local search methods. The latter operate within the EA-loop. This is called “memetic algorithms”, introduced by Moscato [26]. Local search can be considered as a form of lifelong learning. BMA starts by creating an initial population, generating Nbact random individuals, where Nbact is the number of bacteria in each generation. In the iteration phase of the algorithm, the bacterial mutation, local search and gene transfer operations are performed until the required number of generations (Ngeneration) is reached.

All evaluations are based on the integral of the square of the error. In this case, the BMA minimizes the cumulative error between the output of the measured training data and the output of the model with the parameters encoded in each bacterium. These meta-parameters are chosen according to the size of the problem to strike a balance between the required computation time and the residual error of the estimate. Parameter settings are derived from preliminary experiments based on experience from previous applications of BMA to other problems [33,34].

1.5. Brief overview of tensor product based polytopic models

The main reason we use this approach is that the resulting model can be used for other applications, such as controller design. The goal of this technique is to get a polytopic model using only an input dataset. The method consists of three main steps. First, a polytopic structure is derived. Then the components are transformed to be the vertices of a convex hull by convex transformation. At the last step the weighting functions are reconstructed numerically. A detailed explanation of the method can be found in [36–41] and in [42].

1.6. Objectives of this paper

The study has two main objectives. First, our goal is to develop accurate, steady-state, data-driven models that describe the TEG’s output power as a function of the cold-side temperature, the hot-side temperature, and the load current. Second, our goal is to compare three model structures suitable for different engineering applications: a compact and easily interpretable parametric model, a fuzzy model suitable for high-precision nonlinear approximation, and a control-oriented polytopic model based on TP transformation. Accordingly, the contribution of this work lies not only in identifying three different models from the same measurement database, but also in evaluating and comparing their accuracy, complexity, and intended application areas within a unified framework, see Table 1.

1.7. Structure of this paper

The structure of this study is as follows. Section 1 presents the background of the subject area, the literature on TEGs, and the objectives of the research. Section 2 describes the modeling task, the structure of the measurement data, and the main challenges of the system under investigation. Section 3 discusses the measurement system, the experimental setup, and the measurement database used in detail.

Subsequently, Section 4 presents the application of the Bacterial Memetic Algorithm. The description and validation of the parameter-based model are presented in Section 4.1, while the structure, training, and validation of the fuzzy model are described in Section 4.2. The TP-model’s transformation-based polytopic approach is presented in Section 5. A comparative evaluation of the three modeling methods is provided in Section 6. Finally, following a section summarizing the limitations, Section 8 summarizes the most important results and conclusions of the study.

2. Problem statement

The objective of this study is to develop accurate data-driven models of a TEG based on steady-state measurement data, where each model

Table 1
Comparison of the three data-driven TEG models in terms of purpose, advantages, limitations, and intended application.

Model	Main output	Main advantage	Main limitation	Intended use
Parametric BMA-based model	$P_{\mathrm{TEG}}(T_c, T_h, I)$ via compact auxiliary V_{TEG} and R_{TEG} terms	Low parameter count and interpretable structure	Requires an assumed functional form	Compact representation and analysis of parameter effects
Fuzzy BMA-trained model	Direct mapping $(T_c, T_h, I) \rightarrow P_{\mathrm{TEG}}$	Highest interpolation accuracy on the measured domain	High complexity, longer training time, and possible overfitting risk	Accurate nonlinear approximation and possible inverse mapping
TP/polytopic model	Control-oriented polytopic approximation	Structured form suitable for future control-oriented formulations	Requires a complete tensor grid and may be sensitive to data completion	Future controller-oriented modeling and structured system representation

has a unique benefit. Due to the strong nonlinearity and temperature dependence of key characteristics—such as internal resistance and terminal voltage—traditional modeling approaches often fail to represent the system with sufficient accuracy.

The primary goal is to construct models that reproduce the input-output characteristics of the TEG accurately and are suitable for use in subsequent design or control tasks.

In the initial step of our methodology is the generation of a dataset through measurements, where the input signals are: cold side temperature $T_c[i]$ $i = 1, 2 \ldots N_{Tc}$, hot side temperature $T_h[j]$ $j = 1, 2 \ldots N_{Th}$ and current $I[k]$ $k = 1, 2 \ldots N_I$. The corresponding measured output is: the power $P[i, j, k]$. The number of input data $N_{Tc} + N_{Th} + N_I$. The number of measured data $N_{Tc} \cdot N_{Th} \cdot N_I$. This dataset subsequently serves as the basis for the data-driven modeling.

Measurements were conducted under steady-state conditions following the thermal and electrical stabilization phase, while dynamic transients are not considered in this study. To address this, a measurement-based modeling framework is adopted, consisting of three parallel approaches:

1. A parametric model, where the electrical behavior is described using fitted analytical expressions. Here the effect of parameter changes can be examined
2. A fuzzy model, in which the geometry of the fuzzy sets is determined directly from data. This is the most accurate model among the three approach, and it can be inverted.
3. A TP model transformation based approach, where at the end, we get a polytopic model from the system. In this case, the polytopic model can be used for controller desing.

In the first two cases, the BMA is used for parameter identification—either to fit the parametric equations or to optimize the fuzzy rule base and membership functions. An overview of the processes can be seen in Fig. 1.

3. Description of measurement

During the operation of electrical devices, energy losses predominantly occur as heat. Effective thermal management is essential to maintain device performance and longevity. TEGs provide a solution by converting waste heat into electrical energy, thereby improving system efficiency while aiding in heat dissipation.

3.1. Experimental setup

To evaluate TEGs, a controlled test system was designed to maintain hot and cold side temperatures between 0–300°C. It includes a 450 W

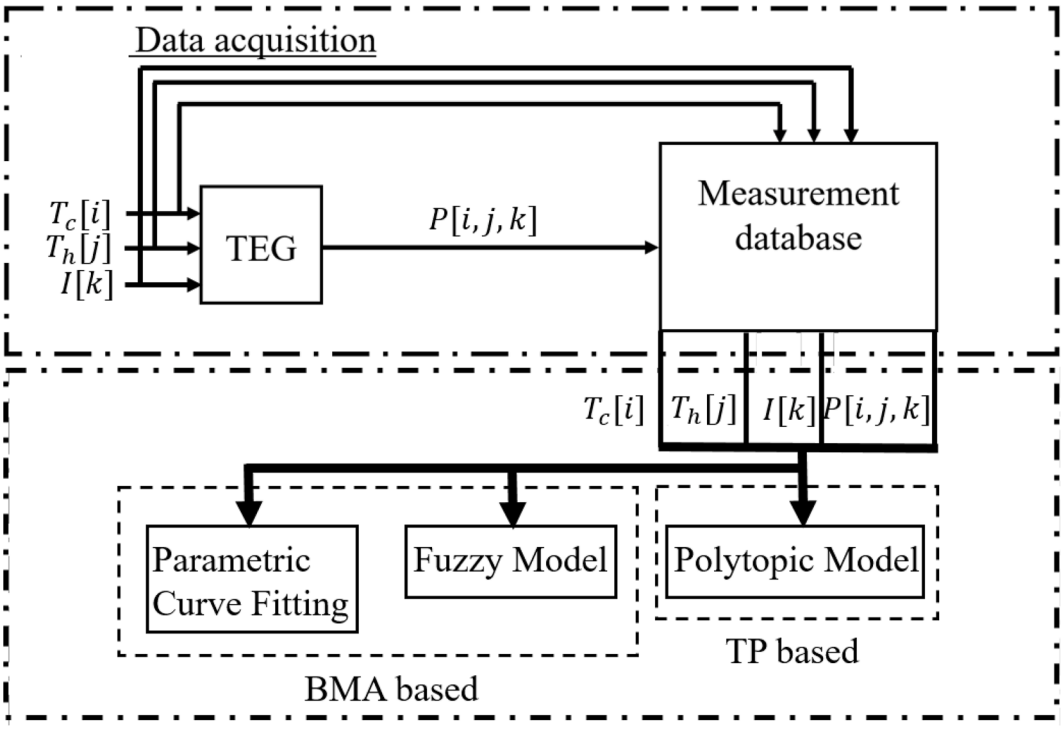

Fig. 1. Overview of data acquisition and model creation.

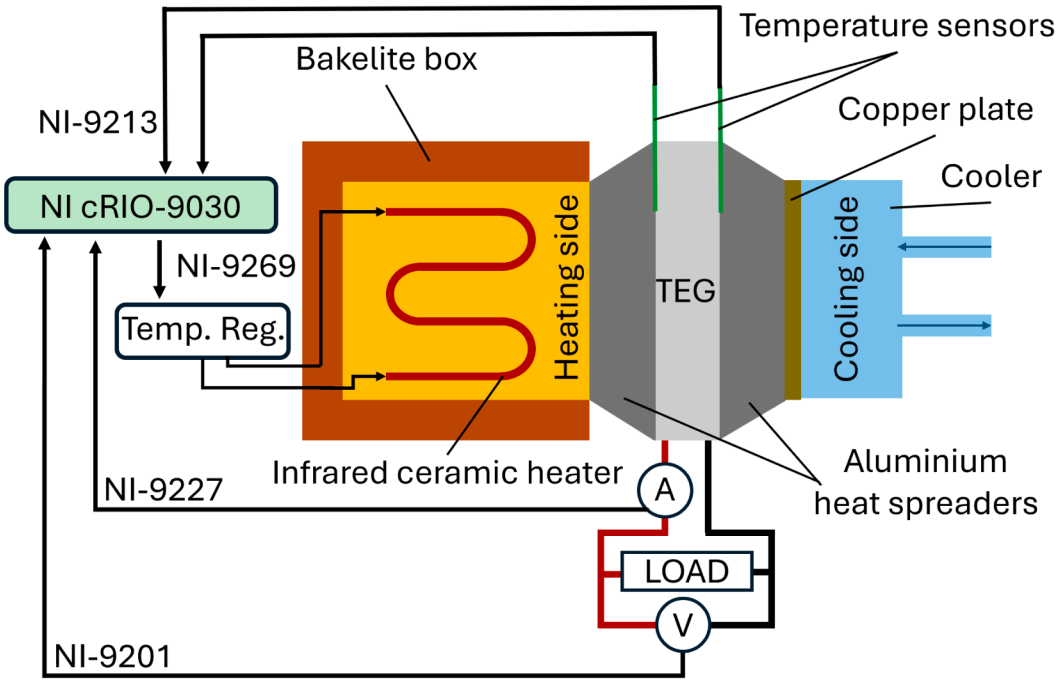

Fig. 2. Structure of the TEG experimental measurement device.

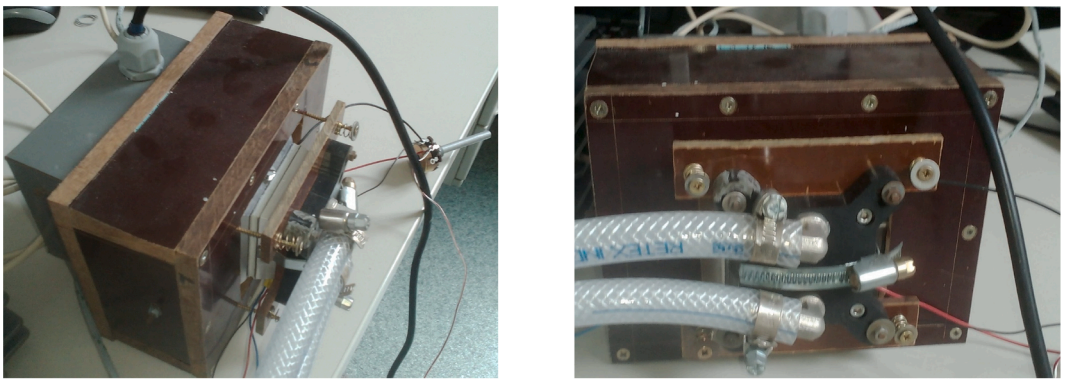

Fig. 3. The actual device.

infrared ceramic heater, a double-insulated bakelite enclosure, and a modular aluminum heat spreader for uniform temperature distribution. The cold side is cooled via a flow-through system with a K-type thermocouple for precise temperature measurement. A detailed schematic of this setup is shown in Fig. 2 and the real-life measurement setup in Fig. 3.

The test system consists of a heated side and a cooled side to maintain a controlled temperature gradient across the TEG. The heated side features a 450 W infrared ceramic heater enclosed within a double-insulated bakelite structure, while the cold side is cooled via a flow-through cooling pad with a mains water connection. K-type thermocouples are integrated on both sides for precise temperature monitoring, ensuring uniform heat distribution across the TEG module.

The 2411G-7L31-15CX1 TEG was chosen as the basis for the measurements [43].

3.1.1. Measurement setup

To evaluate TEG performance, a National Instruments (NI) Compact series measurement and control system was employed. The setup consists of multiple modules, each responsible for specific measurement tasks. The list of the modules can be seen in Table 2.

3.1.2. Heating control system

The heating unit is regulated through a triac control circuit, incorporating opto-triac galvanic isolation to protect the control output module. The triac is fired using a phase-angle control method, ensuring precise temperature regulation. The heating element operates at 230 V_{AC}, and the control signal is generated by a software-based PID module. The PID controller utilizes a temperature-difference-based control strategy, producing a PWM-modulated square wave synchronized with the 50 Hz mains frequency. After testing the no-load parameters, operating point determination measurements were planned. The TEG operates in a operating point condition when its internal resistance is equal to the value of the load resistance connected to it. To determine the operating point parameters, the value of the internal resistance of the TEG is necessary.

To fully understand the module, we made validation measurements, where the measurement system was unchanged, only the TEG output terminals were connected to a precision high-power potentiometer, which can vary its resistance between 0–5.5 Ω. Measurements were performed in 0.1 Ω steps for accurately held temperature differences. The result of the test show that a module can produce about 2.7 W of electrical power at a difference of nearly 200°C.

Table 2
Measurement and control modules.

Module	Specification	Function
NI-9213	16-channel, 24-bit thermocouple module	Measures hot and cold side temperatures
NI-9201	±10 V, 500 kS/s, 12-bit, 8-channel AI module	Measures TEG output voltage
NI-9227	50 kS/s/ch, 0–5 Arms, 24-bit, 4-channel AI module	Measures TEG output current
NI-9269	100 kS/s/ch, ±10 V, 4-channel AO module	Generates control signals for temperature regulation

3.1.3. Measurement dataset

Measurements were performed on a structured operating grid. The cold-side temperature was measured in the following points $T_c \in [25, 30, 35, 40, 50, 60]\,°C$, resulting in $N_{Tc} = 6$ levels. The hot-side temperature was measured in the following points $T_h \in [50, 60, 80, 105, 130, 160, 200, 260]\,°C$, resulting in $N_{Th} = 8$ levels. The load current was varied in the range $I \in [0.09, 1.85]\,A$, resulting in $N_I = 397$ levels. The total number of operating points in the dataset was $N = 1191$, since measurements were not taken for every combination of cold side and hot side temperatures. At each operating point, the data were recorded only after thermal and electrical steady state had been reached.

4. Implementation of bacterial memetic algorithm

The BMA is a hybrid optimization approach combining the global search capability of evolutionary algorithms with the precision of gradient-based local search methods, specifically the Levenberg-Marquardt (LM) algorithm, the pseudo-code of BMA shown in Algorithm 1, an overview can be seen in Fig. 4. This combination allows for robust parameter identification, particularly in systems characterized by non-linear, non-continuous behavior.

Algorithm 1 Bacterial memetic algorithm for TEG parameters identification.

Require: Training set form TEG measurement: $T_c[i], T_h[j], I[k], P_{TEG}(T_c[i], T_h[j], I[k])$
where $i = 1 \ldots N_{Tc}$ $j = 1 \ldots N_{Th}$ $k = 1 \ldots N_I$
Require: Global parameters: N_{bact}, $N_{generation}$,
Create initial population including N_{bact} bacteria
for $gen = 1$ to $N_{generation}$ **do**
  for $bac = 1$ to N_{bact} **do**
    Bacterial mutation algorithm
    Selection the best bacterium
      including Algorithm 2, 3 Evaluation
    Local search using Levenberg-Marquardt method
      including gradient calculation
  Gene transfer in the population
    including Algorithm 2, 3 Evaluation

The BMA operates through three main phases: bacterial mutation, local search, and gene transfer. Each phase contributes to refining the solutions within the population, ensuring both exploration of the search space and exploitation of promising regions. These phases are further supported by an evaluation mechanism, which assesses the fitness of each solution in the context of the optimization problem. The bacterial mutation, Levenberg-Marquardt, and gene transfer algorithms are described in detail in a separate publication, which we reference here [27].

Fundamentally, the system identification is carried out through two distinct approaches. First we set up (1) and (2) parametric equations, which contain 3 input parameters and 8 parameters which should be identified. Additionally, a fuzzy model is constructed, in which both the Antecedent sets $A_{i,j}$ and the consequent Sets B_i are defined using trapezoidal membership functions (TMF). Consequently, the identification task involves determining the anchor points of the trapezoidal vertices. The detailed description of the fuzzy model training process is presented in Section 4.3.

The engineering step, where the objective is to minimize the Sum of Squared Error (SSE) in order to identify the optimal model parameters is in the Evaluation. During this phase, each bacterium is evaluated by a fitness function that quantifies its performance. Specifically, the fitness function calculates the squared error at each simulation step—defined as the square of the difference between the measured (real) value and the simulated (calculated) value—and accumulates it into the total error function $E_{SSE}(\mathbf{b}_i)$. This cumulative error represents the bacterium's fitness, guiding the optimization process. While the general algorithmic structure is outlined here, the specific implementations for the parameter identification tasks can be found in Algorithm 2.

Algorithm 2 Evaluation of fitness function for power.

Require: Retrieved training set: $P_{TEG}(T_c[i], T_h[j], I[k])$ where $i = 1 \ldots N_{Tc}$ $j = 1 \ldots N_{Th}$ $k = 1 \ldots N_I$
Require: Parameter set: $\mathbf{b}_i$
Require: Numerical model: Equation (2) and inputs of T_c, T_h and I
set $E_{SSE}(\mathbf{b}_i) = 0$
for $i = 1$ to N_{Tc} **do**
  for $j = 1$ to N_{Th} **do**
    for $k = 1$ to N_I **do**
      Calculate one integral step by numerical model
      Calculate the error square of the simulation step
      Add the error square of the simulation step to $E_{SSE}(\mathbf{b}_i)$

We selected the BMA hyperparameters based on preliminary tuning runs to strike a balance between the sum of squared errors (SSE) and the corresponding computation time. In particular, we gradually increased the parameters N_{bact}, N_{gen}, and N_{clones}, as well as the number of Levenberg-Marquardt (LM) iterations, until the improvement in the median SSE during repeated runs was negligible. Accordingly, the final parameter settings were chosen based on a trade-off between estimation accuracy and computational cost. We do not claim to have achieved a guaranteed global optimum; instead, we empirically examined convergence by tracking the evolution of the best and median SSE values across iterations, as well as by repeatedly running the optimization from multiple, different random initializations.

4.1. Parameter identification of the thermoelectric generator measurements

Using the measurement data of the TEG, we can combine the measurements of the internal resistance (R_{TEG}), the output voltage (V_{TEG}) and the load current (I) with the input data of our measurements, known as cold-side, hot-side temperatures and the current (T_c, T_h, I).

In this study, the common target variable of all three modeling approaches is the measured output power, denoted by P_{TEG}. In the parametric model, the temperature-dependent voltage and internal resistance terms, V_{TEG} and R_{TEG}, are introduced only as auxiliary latent quantities to construct a compact analytical expression for power according to $P_{\text{TEG}} = \left(V_{\text{TEG}} - I \cdot R_{\text{TEG}}\right) \cdot I$. Therefore, the parametric, fuzzy, and TP-based models are all formulated and compared on the same measured output quantity, namely P_{TEG}.

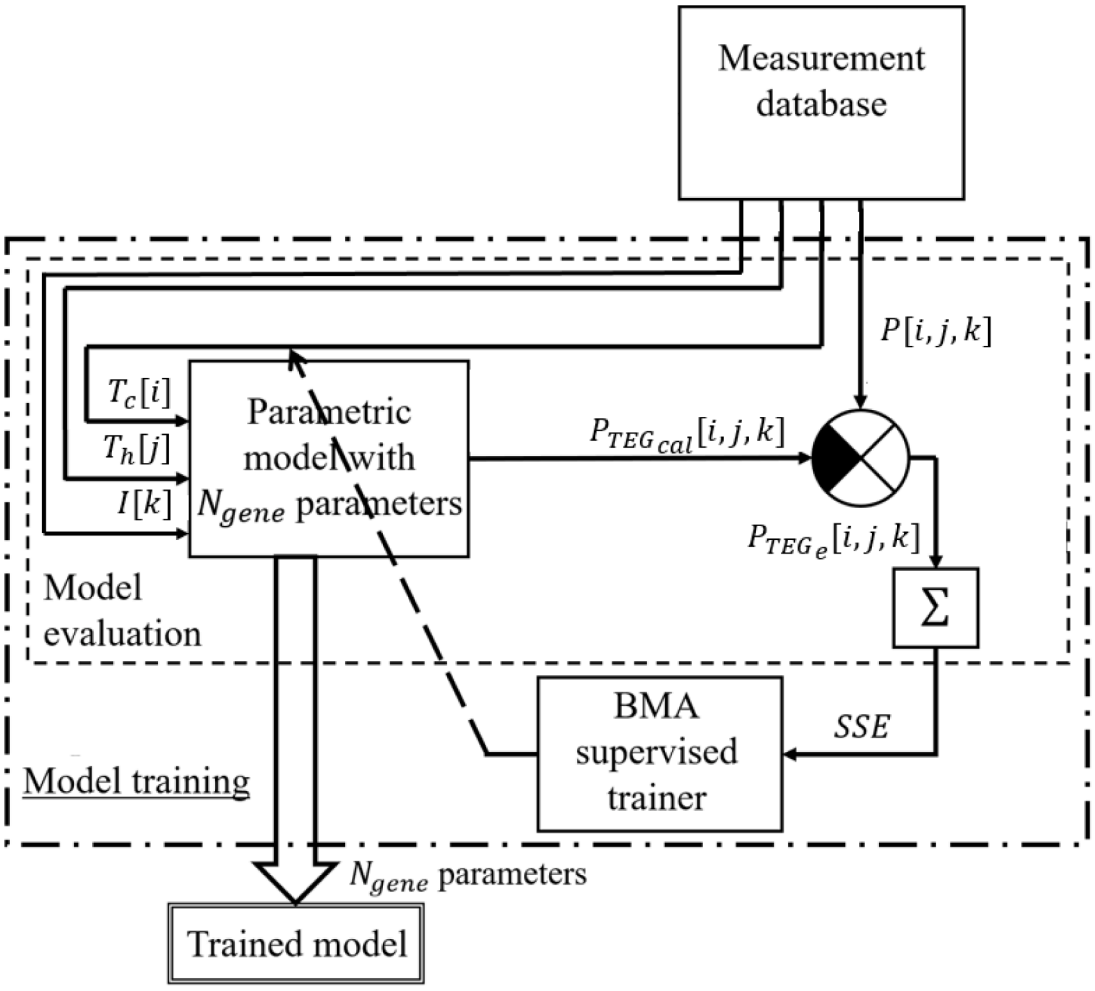

Fig. 4. Overview of BMA model training.

The structure of the parametric model is semi-empirical and was determined based on an analysis of the measured operating point curves. Within the examined range, the effect of the hot-side temperature exhibited a monotonically increasing trend with a saturation behavior, which justified the use of an exponential saturation term. In contrast, the dependence of the cold-side temperature was approximately linear within the examined interval; therefore, to preserve the model's compactness and identifiability, a linear correction term was applied. The model structure developed in this way is thus based on a thermoelectric differential equation model that is supported by physical considerations, yet data-driven, and not derived from first principles.

In TEG systems, accurately modeling the power of the device (P_{TEG}) is crucial for optimizing performance and efficiency. The relationship between the power and operating temperatures—both the hot-side temperature (T_h) and the cold-side temperature (T_c)—is non-linear and varies significantly with different thermal gradients. After analyzing the characteristics of the TEG from the experimentally measured curves, we determined the following Eqs. (1) and (2) for the parameter identification, where the parameters and their behavior on the system is listed afterwards.

$$P_{TEG} = (V_{TEG_{cal}} - I \cdot R_{TEG_{cal}}) \cdot I \tag{1}$$

which can be rewrite as follows:

$$P_{TEG} = (V_0 + Vin_h \cdot (1 - e^{(V_{exp} \cdot T_h)}) - Vin_c \cdot T_c - I \cdot (R_{I0} + Sl_h \cdot (1 - e^{(R_{exp} \cdot T_h)}) - Sl_c \cdot T_c)) \cdot I \tag{2}$$

Where the parameters are:

- V_0: Constant part of the generator voltage independent of temperature
- Vin_h: Parameter defining the slope of the line linearly modeling the dependence of the terminal voltage on the hot spot temperature
- V_{exp}: Parameter defining the saturation of the temperature dependence of the terminal voltage described by an exponential function
- Vin_c: Parameter defining the slope of the line line linearly modeling the dependence of the terminal voltage on the cold spot temperature
- R_{I0}: The temperature independent constant part of the internal resistance
- Sl_h: The parameter determining the slope of the line that linearly models the dependence of temperature on the hot point of the internal resistance
- R_{exp}: The parameter determining the saturation of the temperature dependence of the internal resistance described by an exponential function
- Sl_c: Parameter determining the slope of the straight line that linearly models the temperature dependence of the internal resistance from the cold spot

Our validation focuses on how (2) can be accurately reproducing the results for the measurements we own, with the parameters that are identified.

The input (obtained from measurement) variables:

- T_c: Cold side temperature
- T_h: Hot side temperature
- I: Current of the TEG

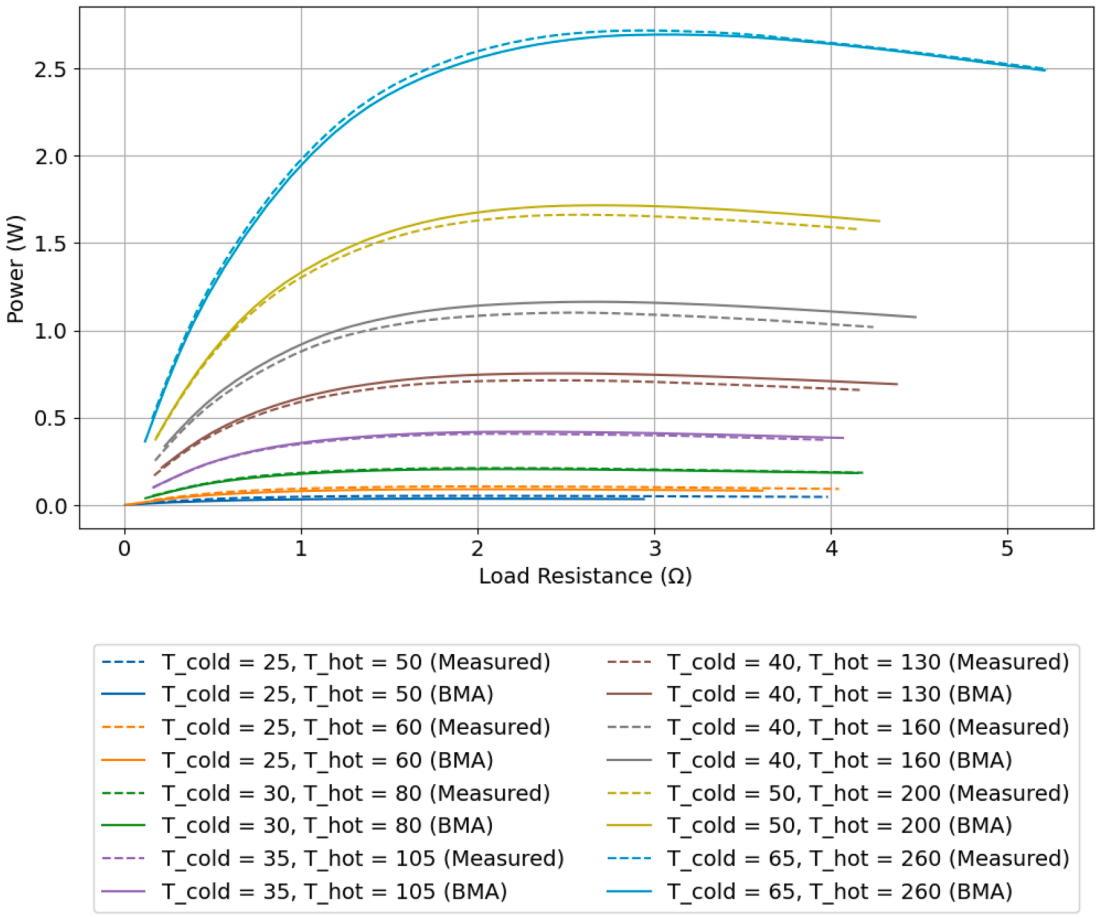

Fig. 5. Validation result of TEG.

The validation equation with the identified parameters:

$$P_{TEG} = (-0.293069 + 134.616382 \cdot (1 - e^{((-0.00021)\cdot T_h)}) - 0.025004 \cdot T_c - I \cdot (1.25 + 1.92 \cdot (1 - e^{((-0.0079)\cdot T_h)}) - (-0.0021) \cdot T_c)) \cdot I \quad (3)$$

Fig. 5 illustrates the validation of the TEG. From the figure it can be seen that the results obtained from the parametric equation identified from the experimental measurement dataset follow very closely the characteristics obtained from the operating point measurements. To compare the data series, we used the R^2 function with a value of 0.99454416, i.e. 99.5%.

The equation has 8 parameters whose values can be learned by machine learning. The equations identified from the characteristics in the measurement results using the BMA approximate the measured values with greater than 99% agreement.

4.2. Data-driven modeling: Determining the validation measurement using fuzzy model

In the previous Section 4.1, we introduced the parametric equations of P_{TEG}. In this section, our goal is to develop a fuzzy model to compute the validation measurement, where the model has three input variables: T_c, T_h, and I, and one output variable, P_{TEG}.

For all three inputs and the output, trapezoidal membership functions are defined. Each membership function is described by four parameters. In the rule base, each rule defines which output membership function corresponds to a given combination of three input membership functions. The training process aims to identify the anchor points of both the input and output membership functions.

To operate the fuzzy model, we apply inference and defuzzification using the well-known Mamdani method [44].

Compared to the earlier case shown in Fig. 5, the key difference is that we no longer optimize the parameters of an equation, but instead identify the anchor points of the membership functions. To describe the model, we define N_{rule} fuzzy rules. Each rule is associated with 4×3 parameters to be identified (see Fig. 6).

In the initial experiment, we generated 49 fuzzy rules. Thus, the optimization process had to identify the parameters for all 49 rules, resulting in bacteria composed of $49 \times 4 \times 4$ parameters, as illustrated in Fig. 6.

As in the previous case, evaluation is performed by comparing the calculated and measured values at each data point. The total error is computed as the sum of squared differences over the entire measurement dataset, which we aim to minimize during optimization.

Due to the nature of fuzzy modeling, where the anchor points of the membership functions must be identified, a large number of parameters is required. The more accurate the model we aim to build, the more rules must be used, which in turn increases the training time.

4.3. Bacterial memetic algorithm for training fuzzy systems

In order to define the fuzzy systems for the TEG validation model, we applied the BMA as a supervised trainer (Fig. 4) on the $N_{patterns}$ training patterns [27]. In this case, the BMA is performing the minimization of the cumulative error between the output of the training patterns and the output of the fuzzy rule bases, by adjusting the breakpoints of the fuzzy rules' trapezoids, encoded into the bacteria. The pseudo-code of the BMA method is shown in Algorithm 1, and the applied meta parameters are listed in Table 3. Most of these parameters are selected

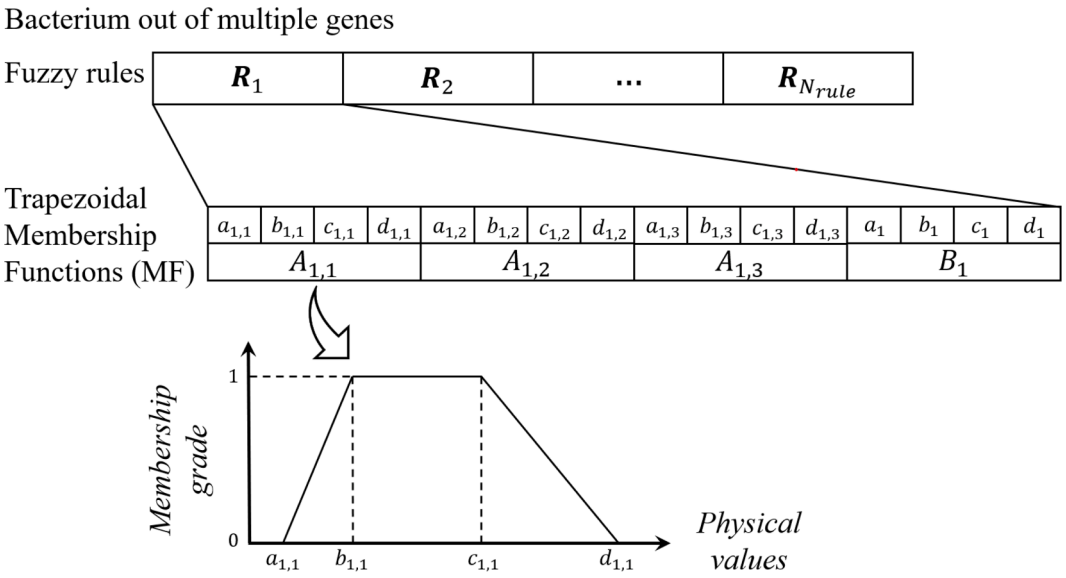

Fig. 6. Each fuzzy rule with trapezoidal membership functions for the 3 inputs (T_c, T_h, I) and 1 output (P_{TEG}), where $a_i < d_i$ and $b_i < c_i$, but no other constraints.

Table 3
Parameters of the TEG validation fuzzy model.

Parameter Name	Value	Parameter Name	Value
$N_{patterns}$	397	N_{ind}	4
N_{rule}	49	N_{gen}	80
M_{unit}/M_{type}	point/1	N_{clones}	25
LM_{prob}	101	l_{bm}	1
γ_{init}	1	LM_{iter}	8
N_{inf}	10	τ	0.0001
l_{gt}	1	I_{unit}	rule

on the basis of practical experience, obtained during the identification process. Determining the optimal parameters is not the scope of this study.

The operation of the BMA starts with the generation of the initial population, generating N_{ind} random individuals with the restriction to maintain the trapezoidal characteristics of the membership functions in the fuzzy rules. The total number of the created membership functions is $N_{ind} \cdot (k+1) \cdot N_{rule}$ where $k = 3$ is the number of input variables and each membership function has four parameters.

Next, in the iteration phase, the bacterial mutation, local search, and gene transfer operations are performed until the termination condition is fulfilled, which is the number of generations (N_{gen}). The bacterial mutation is applied one by one to each bacterium. First, N_{clones} clones of the rule base are generated, which are then subjects of random changes in their genes according to the mutation unit (M_{unit}), which can either be a breakpoint of the trapezoid, or an entire trapezoid, or an entire rule. The number of genes that are modified during this mutation is given by the mutation segment length (l_{bm}) parameter of the algorithm. The best individual transfers the mutated part into the other individuals. In the end, only the best rule base is kept. The evaluation of the fitness function can be seen in Algorithm 3.

4.4. Validation results of the fuzzy model

Regarding the Fig. 5 our goal was to use the two already identified model trained with two separate sets of measurements, combined in Eq. (3) to validate the behaviour of the combined TEG model. In contrast, here we tried to learn this complex measurement directly. Our goal with this was to obtain a model which in the future can be used to made an inverse model of the TEG device.

Algorithm 3 Evaluation of fitness function for fuzzy sets.

Require: Retrieved/measured training set: $T_c(i), T_h(j), I(k)$ and P_{TEG} where $i = 1 \ldots N_{Tc}$ $j = 1 \ldots N_{Th}$ $k = 1 \ldots N_I$
Require: Parameters of the fuzzy model: $N_{patterns}, N_{rule}, N_{gen}, N_{bact}$ and N_{clone}, all listed in Table 3
set $E_{SSE}(\mathbf{b}_i) = 0$
for $i = 1$ to N_{Tc} **do**
  for $j = 1$ to N_{Th} **do**
    for $k = 1$ to N_I **do**
      Calculate the error square of the simulation step
      Add the error square of the simulation step to $E_{SSE}(\mathbf{b}_i)$

We can see on the Fig. 7, that the fuzzy model result show improved agreement with the measured data. Based on the coefficient of determination (R^2), which quantifies the proportion of variance in the measured data explained by the model predictions, the performance of the BMA and fuzzy approaches was evaluated. The corresponding R^2 value for BMA is 0.99454416, i.e. 99.5%, compared to the fuzzy model value of 0.99923320, i.e. 99.9%. The parameters used to train the fuzzy model can be seen in Table 3, according to that 49 rule bases were needed to get this high accuracy. These results highlight the relative predictive accuracy of each method with respect to the experimental measurements, providing a quantitative basis for model comparison.

5. Tensor product (TP) modeling

Our third approach to make a model for the TEG device is based on the TP model transformation. The aim of this is that as a result a polytopic model is obtained in state-space form, which can be easily used for controller design in contrast to the previous two model. An overview of the process can be seen in Fig. 8. Based on the measurement, the power of the TEG was determined as a function of the cold and hot side temperatures, as well as the TEG's current, using a three-variable function $f_o(T_c, T_h, I)$:

$$P_{TEG} = f_o(T_c, T_h, I) \tag{4}$$

Once we are in possession of the data, the question is that the measured dataset is large enough to get the essential information to make the data based model. Analyzing the structure of the measurement data

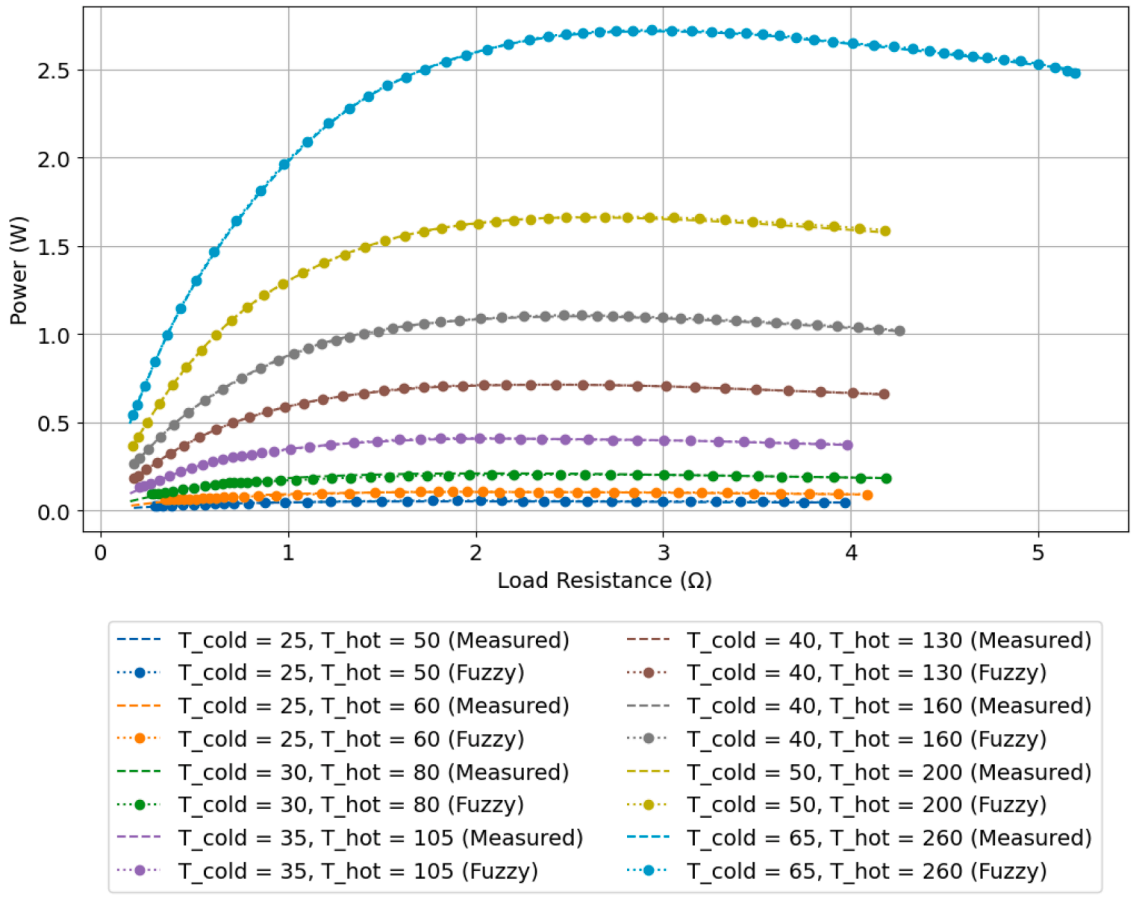

Fig. 7. Comparison of the measurement data, identified combined parametric equation and fuzzy model.

with singular value decomposition (SVD) will answer the question. With SVD we would like to get the redundant information from the dataset. As discussed above the dataset have three input values T_c, T_h and I. The whole matrix can be seen in Fig. 9 where *md* represents the measured data. i is the number of measured cold side temperatures, j is the number of measured hot side temperatures and k is the number of measured current values.

The process require a fully filled matrix. Since we don't have enough measurement values to get each *md* in Fig. 9, we will fill in the missing data using the model obtained in Section 4.3.It is important to note that helper variables are only necessary for running the algorithm. They do not affect the model within its operating range of the TEG.

Based on Fig. 9 we get a $i \times j \times k$ dataset with measured values. Using the SVD on this matrix we will get the following set of matrices Fig. 10.

Fig. 10 can be rewrite as

$$\mathbf{M}_d = \mathbf{U}\boldsymbol{\Sigma}\mathbf{V}^{\mathbf{T}} \tag{5}$$

Our experience is that if we measure at several hundred or several thousand points, only a few of the σ singular values are different from zero. Thus, in the (5) matrix multiplication, we perform many unnecessary operations, because we multiply by zero. If we omit the rows and columns whose multiplication results in zero, we get a significantly simpler structure. This can be explained by the fact that the behavior of the system can presumably be described by a system of differential equations consisting of a few equations, but in this approach we are not looking for the system of differential equations but for the relationships of the measured data in the following form.

$$\mathbf{M}_d(T_c, T_h, I) = \sum_{i=1}^{N_c}\sum_{j=1}^{N_h}\sum_{k=1}^{N_I} w_{Tc,i}(T_c) w_{Th,j}(T_h) w_{I,k}(I) m_{i,j,k}, \tag{6}$$

where

$$\forall (T_c, T_h, I) : \mathbf{M}_d(T_c, T_h, I) \in co\{\forall i, j, k : m_{i,j,k}\}. \tag{7}$$

In other words, $m_{i,j,k}$ are the vertices of a convex shape containing all measured results (see (7)). Furthermore, using the vertices of this convex shape and the weight function $w_{Tc,i}(T_c), w_{Th,j}(T_h), w_{I,k}(I)$, any measurement point can be reconstructed based on (6). The $m_{i,j,k}$ vertices and weight functions can be chosen in several different ways, but for other reasons, the following is a reasonable choice:

$$\forall T_c : \sum_{i=1}^{N_c} w_{Tc,i}(T_c) = 1; \quad \text{and} \quad \forall i, T_c : 0 \le w_{Tc,i}(T_c). \tag{8}$$

$$\forall T_h : \sum_{j=1}^{N_h} w_{Th,j}(T_h) = 1; \quad \text{and} \quad \forall j, T_h : 0 \le w_{Th,j}(T_h). \tag{9}$$

$$\forall I : \sum_{k=1}^{N_I} w_{I,k}(I) = 1; \quad \text{and} \quad \forall k, I : 0 \le w_{I,k}(I). \tag{10}$$

It can be seen that only the measured values corresponding to discrete temperature and current values can be read from the Fig. 9 matrix, whereas the formula (6) calculates a value for any pair of temperatures and current within a given range.

For the process we used Sum-normalized and Non-negative (SNNN) normalization method [39]. Using and testing other normalization methods is not the scope of this paper. Originally we had $6x6x264 = 9504$

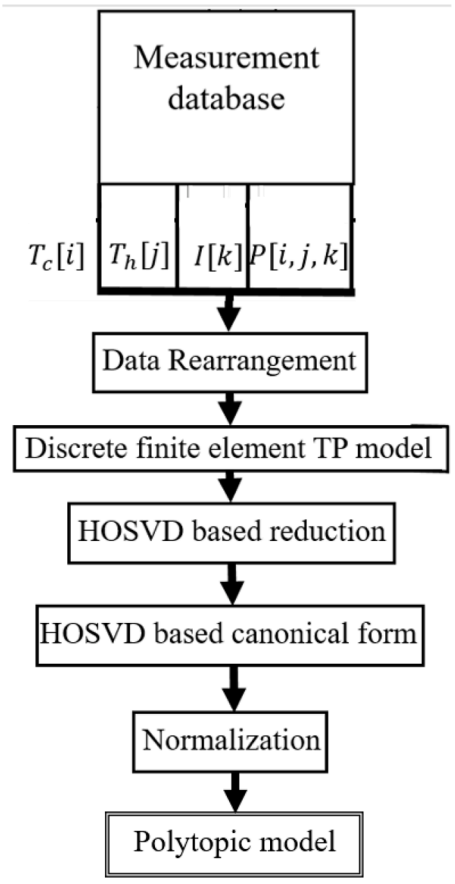

Fig. 8. Overview of the TP model transformation process.

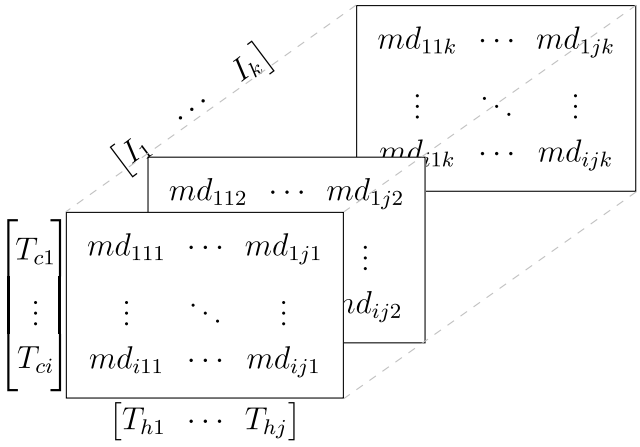

Fig. 9. Representation of the measured dataset.

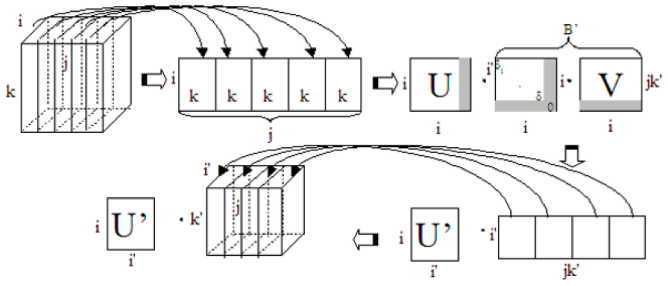

Fig. 10. Visualization of HOSVD.

grid points and that number is reduced to $3x3x3 = 27$ vertex points by HoSVD. The resulted vertex points $m_{i,j,k}$ are arranged in a form of Fig. 9 and they can be seen in (11), (12), (13). With the calculated vertex points $m_{i,j,k}$ and the corresponding weighting functions shown in Fig. 11, the results received from the model compared to the measurement results in Fig. 12.

$$M_{I_1} = \begin{bmatrix} -3.0217 & -4.1274 & 9.8276 \\ -0.0990 & -0.1353 & 0.3221 \\ 0.3783 & 0.5167 & -1.2303 \end{bmatrix} * 10^7 \tag{11}$$

$$M_{I_2} = \begin{bmatrix} 0.8442 & 1.1530 & -2.7454 \\ 0.0277 & 0.0378 & -0.0900 \\ -0.1057 & -0.1443 & 0.3437 \end{bmatrix} * 10^7 \tag{12}$$

$$M_{I_3} = \begin{bmatrix} -1.0420 & -1.4227 & 3.3886 \\ -0.0342 & -0.0466 & 0.1112 \\ 0.1304 & 0.1781 & -0.4241 \end{bmatrix} * 10^5 \tag{13}$$

6. Comparative evaluation of the three modeling approaches

We conducted a comprehensive, power-based statistical comparison between the BMA, fuzzy, and TP models. In addition to the coefficient of determination (R^2), the analysis included the RMSE, MAE, and MBE metrics, 95% bootstrap confidence intervals, and pairwise comparisons of absolute errors using paired t-tests and Wilcoxon signed-rank tests. This expanded evaluation provides a more rigorous and reliable picture of the models' performance than reporting the R^2 value alone.

Table 4 shows the global performance of the three models across all valid, power-based evaluation points. Overall, the fuzzy model provided the best predictive performance, as it yielded the highest R^2 and the lowest RMSE and MAE values. At the global level, the BMA model ranked second, while the TP model showed the weakest overall performance among the three approaches. The global pairwise comparisons presented in Table 5 confirm this trend: the fuzzy model proved to be significantly better than both the BMA and TP models, while the BMA model also performed significantly better than the TP model.

However, a comparison under operating conditions revealed a more nuanced picture. For $T_{cold} = 25°C$ and $T_{hot} = 50°C$, only the BMA and fuzzy models were comparable, and of these, the fuzzy model proved to be significantly better. For the 25/60°C temperature pair, the TP model delivered the best local performance, outperforming both the BMA and fuzzy models. At 30/80°C, the BMA model proved to be the best, significantly outperforming both the fuzzy and TP models, while the difference between the fuzzy and TP models was not statistically significant. For the 35/105°C case, the fuzzy model numerically achieved the smallest MAE value. However, its advantage over the BMA model was not consistently supported by both statistical tests, at the same time, both models clearly outperformed the TP model. At the 40/130°C and 40/160°C operating points, the fuzzy model was the dominant approach, followed by the BMA model, while the TP model yielded the largest prediction errors. In the 50/200°C case, the fuzzy model again performed best, the TP model finished in second place, while the BMA model showed the largest absolute error. Finally, at the 65/260°C extreme operating point, we found no statistically significant difference between the BMA and fuzzy models, while no valid data were available for the TP model at this point. A condition-wise comparison can be seen in Table 6.

Overall, these results show that, in performance-based evaluation, the fuzzy model provides the most robust general predictive framework. At the same time, the BMA model remains competitive within a specific operating range (30/80°C) and even yields better results there, while the TP model can outperform both other data-driven approaches under certain conditions (25/60°C). Accordingly, the comparative analysis suggests that for general-purpose applications, the fuzzy model can be considered the most accurate solution, while the relative advantage of each model depends on the specific operating point.

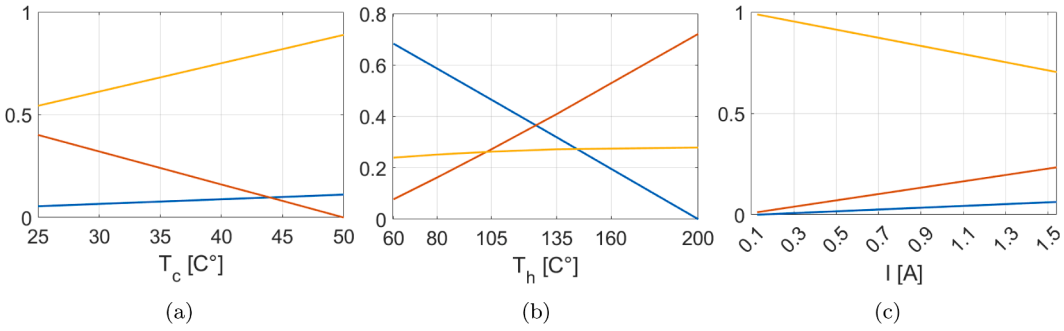

Fig. 11. Weighting functions ($N_c = N_h = N_I = 3$).

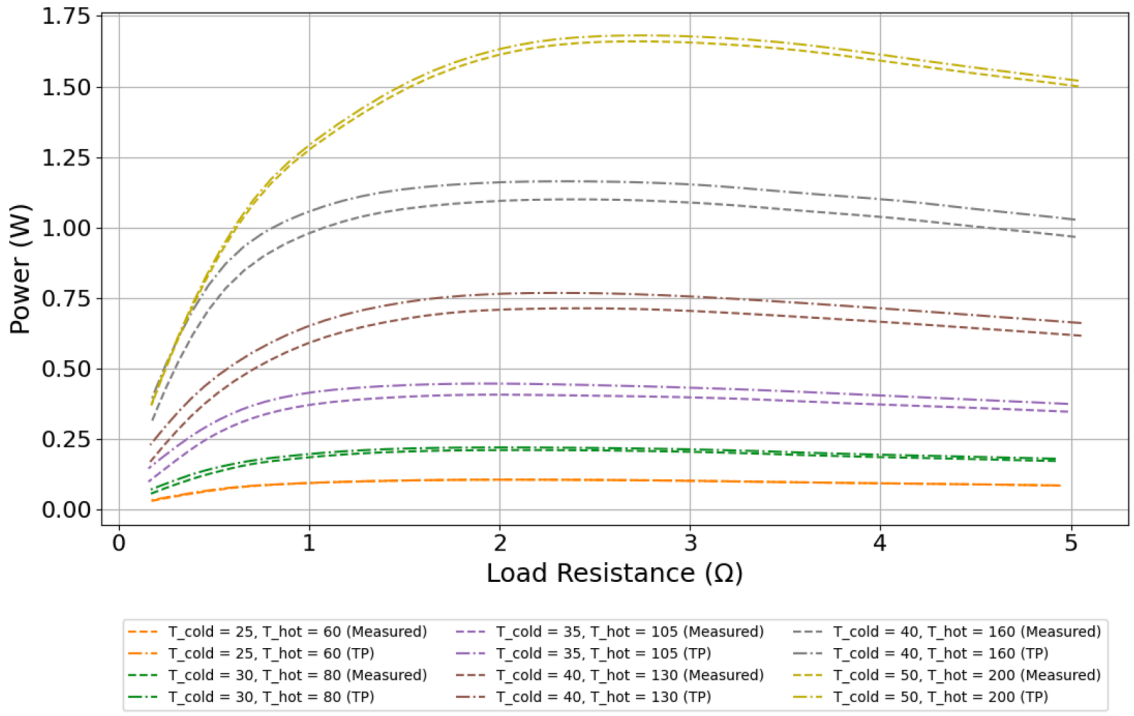

Fig. 12. Comparison of the measured data points, with the data points gathered from the polytopic model.

Table 4
Global power-based statistical comparison of the BMA, fuzzy, and TP models over all valid measurement points.

Model	R^2 [95% CI]	RMSE [95% CI]	MAE [95% CI]	MBE [95% CI]
BMA	0.9976 [0.9969, 0.9980]	0.0399 [0.0370, 0.0428]	0.0309 [0.0285, 0.0334]	0.0096 [0.0058, 0.0133]
Fuzzy	0.9991 [0.9985, 0.9995]	0.0245 [0.0180, 0.0307]	0.0106 [0.0086, 0.0129]	0.0022 [-0.0002, 0.0047]
TP	0.9932 [0.9913, 0.9946]	0.0407 [0.0379, 0.0435]	0.0321 [0.0291, 0.0350]	0.0320 [0.0290, 0.0350]

Table 5
Global pairwise comparison of absolute errors for the three models. Positive values indicate that the second model in the comparison performed better; negative values indicate that the first model performed better.

Comparison	ΔMAE [95% CI]	Paired t-test p	Wilcoxon p	Cohen's d_z
BMA vs Fuzzy	0.0203 [0.0175, 0.0229]	< 0.001	< 0.001	0.746
BMA vs TP	-0.0086 [-0.0130, -0.0046]	< 0.001	0.0030	-0.233
Fuzzy vs TP	-0.0334 [-0.0389, -0.0281]	< 0.001	< 0.001	-0.710

7. Limitations

The study has several limitations. First, all models were identified based solely on measurements taken under steady-state conditions. Therefore, transient thermoelectric dynamic phenomena were not modeled. Second, the fuzzy model contains a relatively large number of free parameters compared to the size of the available dataset, therefore, the favorable fit results should be interpreted in conjunction with independent validation results to reduce the risk of overfitting. Third, the TP model transformation requires a full tensor lattice. For this reason, the final polytopic model depends in part on the data imputation strategy used to fill in missing grid points. In this context, the first and last data series were not included in the TP model, as they are located at the extreme points of the measurement range, where the consistent construction of the full tensor lattice could not be ensured with sufficient reliability. Including these extreme points would have required not only the replacement of missing grid elements but also extrapolation-based estimates, which would have increased the uncertainty of the TP representation. Fourth, the models presented were validated exclusively within the measured operating range, so, their application outside the

Table 6
Condition-wise ranking of the three models in the power-based evaluation.

Temperature pair (T_{cold}/T_{hot})	Best-performing model	Interpretation
25 / 50	Fuzzy	TP unavailable; fuzzy significantly outperformed BMA.
25 / 60	TP	TP outperformed both BMA and fuzzy; fuzzy outperformed BMA.
30 / 80	BMA	BMA outperformed both fuzzy and TP; fuzzy and TP were not significantly different.
35 / 105	Fuzzy (numerically)	Fuzzy had the lowest MAE; superiority over BMA was not consistent across tests; both outperformed TP.
40 / 130	Fuzzy	Fuzzy performed best, followed by BMA; TP was the weakest.
40 / 160	Fuzzy	Fuzzy performed best, followed by BMA; TP was the weakest.
50 / 200	Fuzzy	Fuzzy performed best; TP outperformed BMA.
65 / 260	No significant difference	TP unavailable; no significant difference was found between BMA and fuzzy.

examined temperature and current ranges can be considered valid only on an exploratory basis. Finally, although TP-based representation may be suitable for supporting future control-oriented developments, control design and closed-loop validation fall outside the scope of this study.

8. Conclusion

In this study, we developed and compared three different data-driven approaches for the measurement-based modeling of the steady-state behavior of a thermoelectric generator (TEG). The common target variable in all cases was the TEG's output power, which we described as a function of the cold-side temperature, the hot-side temperature, and the load current. The models were created from the same structured measurement dataset, which contained 1191 steady-state operating points within the examined temperature and current ranges. The fundamental objective of this work was not only to identify three different models, but also to demonstrate that model structures suitable for different engineering purposes can be derived from the same measurement database.

The BMA model, based on parameter identification, provided a compact and easily interpretable analytical description of the TEG's performance. Its advantage is that it uses relatively few parameters, making it suitable for concisely describing the system's main relationships and interpreting the effects of individual parameters. In contrast, the fuzzy model did not require a predefined analytical structure, and its flexible rule base allowed it to track the nonlinear input-output relationship more accurately. The primary strength of the polytopic model based on the TP transformation is not the highest predictive accuracy, but rather the structured, control-oriented representation, which may be advantageous for subsequent control engineering applications. The three approaches are therefore not simply alternatives to one another, but offer different trade-offs between compactness, accuracy, and structural usability.

Based on the overall statistical comparison, the fuzzy model delivered the best overall performance: it achieved the highest coefficient of determination and the lowest RMSE and MAE values ($R^2 = 0.9991, RMSE = 0.0245, MAE = 0.0106$), while the BMA model lagged slightly behind but still showed strong results ($R^2 = 0.9976, RMSE = 0.0399, MAE = 0.0309$). The TP model performed slightly worse overall ($R^2 = 0.9932, RMSE = 0.0407, MAE = 0.0321$); however, pairwise statistical comparisons confirmed that the fuzzy model significantly outperformed both the BMA and TP models, and the BMA was also significantly better than the TP model. These results indicate that the fuzzy model is the most favorable choice for general-purpose, high-precision performance estimation.

However, the analysis of individual operating conditions provided a more nuanced picture. Although the fuzzy model proved to be the strongest general solution, it was not the best at every operating point. For the 25/60 °C temperature pair, the TP model yielded the best local result, while at 30/80 °C, the BMA model performed best. At several other operating points, the fuzzy model remained the leading approach, and in the extreme 65/260 °C case, no significant difference was detected between the BMA and the fuzzy model, while TP data were not available. This means that although the fuzzy model provides the most robust general predictive framework, the relative advantage of each model still depends on the operating range.

Overall, the main finding of the study is that we were able to create three TEG models from the same dataset, each suitable for different purposes, and systematically compare them. The fuzzy model proved to be the best general-purpose predictive solution, the BMA model offered a compact and easily interpretable alternative, while the TP representation is primarily valuable for future control-oriented applications. However, the results presented are valid in their current form only for the steady-state, measured operating range. Future work may include further validation of the models using independent data, analysis of robustness against measurement noise, the impact of imputed data on the TP model, as well as control design and closed-loop validation based on the TP-based representation.

CRediT authorship contribution statement

Károly Árpád Kis: Writing – review & editing, Writing – original draft, Visualization, Software, Investigation; **Kornél Sarvajcz:** Resources, Methodology, Investigation, Data curation; **Róbert Mikuska:** Writing – review & editing, Writing – original draft, Visualization, Software, Investigation; **Péter Korondi:** Writing – review & editing, Supervision, Software, Project administration, Methodology.

Data availability

Data will be made available on request.

Declaration of competing interest

The authors declare that they have no known competing financial interests or personal relationships that could have appeared to influence the work reported in this paper.

Acknowledgment

This research was supported and funded by the Hungarian Research Fund (OTKA K-143595) and by the EKÖP-24-2 University Research Scholarship Program of the Ministry for Culture and Innovation From the Source of the National Research, Development and Innovation Fund.

References

[1] S. Lan, R. Stobart, X. Wang, Matching and optimization for a thermoelectric generator applied in an extended-range electric vehicle for waste heat recovery, Appl. Energy 313 (2022a) 118783.
[2] S. Lan, R. Stobart, R. Chen, Performance comparison of a thermoelectric generator applied in conventional vehicles and extended-range electric vehicles, Energy Convers. Manag. 266 (2022b) 115791.
[3] W.B. Nader, Thermoelectric generator optimization for hybrid electric vehicles, Appl. Therm. Eng. 167 (2020) 114761.
[4] W. Mohamed, B. Singh, M.F. Mohamed, A.M. Aizuwan, A. Zubair, Effects of fuel cell vehicle waste heat temperatures and cruising speeds on the outputs of a thermoelectric generator energy recovery module, Int. J. Hydrog. Energy 46 (50) (2021) 25634–25649.
[5] D. Luo, Z. Sun, R. Wang, Performance investigation of a thermoelectric generator system applied in automobile exhaust waste heat recovery, Energy 238 (2022) 121816.

[6] V. Abbasi, V.S. Tabar, Measurement and evaluation of produced energy by thermoelectric generator in vehicle, Measurement 149 (2020) 107035.

[7] C.C. Sousa, J. Martins, Ó. Carvalho, M. Coelho, A.S. Moita, F.P. Brito, Assessment of an exhaust thermoelectric generator incorporating thermal control applied to a heavy duty vehicle, Energies 15 (13) (2022). https://doi.org/10.3390/en15134787

[8] A. Coulibaly, N. Zioui, S. Bentouba, S. Kelouwani, M. Bourouis, Use of thermoelectric generators to harvest energy from motor vehicle brake discs, Case Stud. Therm. Eng. 28 (2021) 101379.

[9] M. Aljaghtham, E. Celik, Design optimization of oil pan thermoelectric generator to recover waste heat from internal combustion engines, Energy 200 (2020) 117547.

[10] G.G. Dalkiranis, J.H.C. Bocchi, B.B.M. Torres, A.F. Lopeandia, O.N. Oliveira, G.C. Faria, Measurement system to determine the seebeck coefficient and electrical conductivity of thin films, IEEE Trans. Instrum. Meas. 74 (2025) 1–6. https://doi.org/10.1109/TIM.2025.3553254

[11] A.W.W. Atmajaya, P. Suwandono, Add-on energy harvesting of diesel exhaust muffler using thermoelectric generator, J. Sci. Appl. Eng. 6 (1) (2023).

[12] A.G. Olabi, M. Al-Murisi, H.M. Maghrabie, B.A.A. Yousef, E.T. Sayed, A.H. Alami, M.A. Abdelkareem, Potential applications of thermoelectric generators (TEGs) in various waste heat recovery systems, Int. J. Thermofluids 16 (2022) 100249.

[13] A. Khoshnevisan, S. Changizian, M. Raeesi, P. Ahmadi, N. Javani, Thermal analysis of thermo-electric generator systems in hybrid electric vehicles under different operating conditions, J. Therm. Anal. Calorim. 148 (18) (2023) 9649–9659.

[14] T.S.K. Kumar, S.A. Kumar, K.K. Ram, K.R. Goli, V.S. Prasad, Analysis of thermo electric generators in automobile applications, Mater. Today Proc. 45 (2021) 5835–5839.

[15] Z. He, Z. Kong, X. Jin, Z. Que, Z. Xu, Remaining useful life prediction of radioisotope thermoelectric generator using a component-level mechanism-based nonlinear additive wiener process, IEEE Trans. Instrum. Meas. 73 (2024) 1–14. https://doi.org/10.1109/TIM.2024.3470018

[16] M.S. Omar, B. Singh, M.F. Remeli, Motorcycle waste heat energy harvesting using thermoelectric generators, J. Electron. Mater. 49 (2020) 2838–2845.

[17] P. Fernández-Yáñez, V. Romero, O. Armas, G. Cerretti, Thermal management of thermoelectric generators for waste energy recovery, Appl. Therm. Eng. 196 (2021) 117291.

[18] W. Zhu, X. Li, Y. Li, C. Xie, Y. Shi, Two-level energy harvesting strategy for multi-input thermoelectric energy system, Energy Rep. 8 (2022) 4359–4372.

[19] J. Pei, F. Guo, J. Zhang, B. Zhou, Y. Bi, R. Li, Review and analysis of energy harvesting technologies in roadway transportation, J. Clean. Prod. 288 (2021) 125338.

[20] S. Bentouba, N. Zioui, P. Breuhaus, M. Bourouis, Overview of the potential of energy harvesting sources in electric vehicles, Energies 16 (13) (2023) 5193.

[21] S. Bai, C. Liu, Overview of energy harvesting and emission reduction technologies in hybrid electric vehicles, Renew. Sustain. Energy Rev. 147 (2021) 111188.

[22] Z. Dong, H. Xu, F. Liang, C. Luo, C. Wang, Z.-Y. Cao, X.-J. Chen, J. Zhang, X. Wu, Raman characterization on two-dimensional materials-based thermoelectricity, Molecules 24 (1) (2018) 88.

[23] T. Bartz-Beielstein, J. Branke, J. Mehnen, O. Mersmann, Evolutionary algorithms, WIREs Data Min. Knowl. Discov. 4 (3) (2014) 178–195. https://doi.org/10.1002/widm.1124

[24] B. Doerr, F. Neumann, Theory of evolutionary computation: recent developments in discrete optimization, Nat. Comput. Ser. (2020).

[25] N.E. Nawa, T. Furuhashi, Fuzzy system parameters discovery by bacterial evolutionary algorithm, IEEE Trans. Fuzzy Syst. 7 (5) (1999) 608–616. https://doi.org/10.1109/91.797983

[26] P. Moscato, et al., On evolution, search, optimization, genetic algorithms and martial arts: towards memetic algorithms, Caltech Concurr. Comput. Program C3P Rep. 826 (1989) (1989) 37.

[27] J. Botzheim, C. Cabrita, L.T. Kóczy, A.E. Ruano, Fuzzy rule extraction by bacterial memetic algorithms, Int. J. Intell. Syst. 24 (3) (2009) 312–339.

[28] K. Levenberg, A method for the solution of certain non-linear problems in least squares, Q. Appl. Math. 2 (2) (1944) 164–168.

[29] D.W. Marquardt, An algorithm for least-squares estimation of nonlinear parameters, J. Soc. Ind. Appl. Math. 11 (2) (1963) 431–441.

[30] J. Botzheim, Y. Toda, N. Kubota, Bacterial memetic algorithm for offline path planning of mobile robots, Memetic Comput. 4 (2012) 73–86.

[31] K. Balázs, J. Botzheim, L.T. Kóczy, Comparative investigation of various evolutionary and memetic algorithms, Comput. Intell. Eng. (2010) 129–140.

[32] D. Zhou, Y. Fang, J. Botzheim, N. Kubota, H. Liu, Bacterial memetic algorithm based feature selection for surface EMG based hand motion recognition in long-term use, in: 2016IEEE Symposium Series on Computational Intelligence (SSCI), IEEE, 2016, pp. 1–7.

[33] Á. Csík, J. Botzheim, J. Balázs, T. Csoknyai, J.L. Hontvári, Energy and cost optimal design for the reconstruction of residential building envelopes by bacterial memetic algorithms, in: The 6th International Conference on Soft Computing and Intelligent Systems, and the 13th International Symposium on Advanced Intelligence Systems, IEEE, 2012, pp. 1226–1231.

[34] J. Botzheim, P. Földesi, Novel calculation of fuzzy exponent in the sigmoid functions for fuzzy neural networks, Neurocomputing 129 (2014) 458–466.

[35] W.H. Organization, Global Status Report on Road Safety 2018, Nonserial Publication, World Health Organization, 2019. https://books.google.hu/books?id=uHOyDwAAQBAJ.

[36] P. Baranyi, Dual-Control-Design TP and TS Fuzzy Model Transformation Based Control Optimisation and Design, Topics in Intelligent Engineering and Informatics (TIEI, volume 17), Springer book, 2023.

[37] P. Baranyi, Y. Yam, D. Tikk, R.J. Patton, Trade-off between approximation accuracy and complexity: TS controller design via HOSVD based complexity minimization, in J. Casillas, O. Cordón, F. Herrera, L. Magdalena, (Eds.) Studies in Fuzziness and Soft Computing, Vol. 128. in Interpretability Issues in Fuzzy Modeling, Springer-Verlag (2003) 249–277. ISBN: 3-540-02932-X

[38] P. Baranyi, Z. Petres, P.L. Varkonyi, P. Korondi, Y. Yam, Determination of different polytopic models of the prototypical aeroelastic wing section by TP model transformation, J. Adv. Comput. Intell. Intell. Inform. 10 (4) (2006) 486–493. ISSN 1343-0130

[39] P. Várkonyi, D. Tikk, P. Korondi, P. Baranyi, A new algorithm for RNO-INO type tensor product model representation, in: Proceedings of IEEE International Conference on Intelligent Engineering Systems, INES'05, USA,Piscataway, 2005, pp. 263–266.

[40] P. Baranyi, TP-model Transformation-based-control Design Frameworks, Springer, 2016.

[41] P. Baranyi, Y. Yam, P. Várlaki, Tensor product model transformation in polytopic model-based control, CRC press, 2018.

[42] D. Tikk, P. Baranyi, R.J. Patton, J.K. Tar, Approximation capability of TP model forms, Aust. J. Intell. Inf. Process. Syst. 8 (2004) 155–163.

[43] C. Thermoelectric, TEG specification sheet, 2014. datasheet, https://customthermoelectric.com/media/wysiwyg/TEG_spec_sheets/2411G-7L31-15CX1_20140508_spec_sht.pdf.

[44] H. Ying, Y. Ding, S. Li, S. Shao, Comparison of necessary conditions for typical Takagi-Sugeno and Mamdani fuzzy systems as universal approximators, IEEE Trans. Syst. Man Cybern. A Syst. Hum. 29 (5) (1999) 508–514. https://doi.org/10.1109/3468.784177